Dynamic Lung Morphology of Methacholine-Induced Heterogeneous Bronchoconstriction

Ben T. Chen and G. Allan Johnson

Hyperpolarized (HP) ^{3}helium (^{3}He) dynamic MRI was used to investigate airway response in rats following intravenous (i.v.) bolus administration of a contractile agent, methacholine (MCh). The method provides direct visualization of the ventilated regions within the lung. Heterogeneous bronchoconstriction following the i.v. MCh injection was evident using this technique. These ^{3}He dynamic lung images revealed that the inspired fresh air was shunted to the less-constricted regions after the MCh challenge in a similar manner as described by Laplace's relationship for the stability between adjacent alveoli. The airways in the more-constricted regions became nearly closed, resulting in air trapping, while the airways in the less-constricted regions remained effectively open, leading to over-inflation. These data suggest a lung model of airway constriction partitioned into ventilated and nonventilated regions. These nonventilated regions are heterogeneously distributed in the lung and this distribution cannot be deduced from spirometric measurement of the whole lung. We demonstrate that a combination of functional ^{3}He images and anatomical ^{1}H images provide an effective method to diagnose regional lung abnormalities in rats. Magn Reson Med 52:1080–1086, 2004. © 2004 Wiley-Liss, Inc.

Key words: MR imaging; hyperpolarized gas; ventilation shunt; regional lung function; air trapping

The increasing incidence of asthma poses a worldwide health problem (1,2), spurring major efforts to understand the mechanism and treatment of the disease. Measurement of pulmonary mechanics using spirometry has been the most common method to evaluate lung function. Unfortunately, this method can only measure global function of the lung. It is generally believed that measurement of regional ventilation within the lung can provide an early diagnosis of lung dysfunction. Since the late 1960s, ventilation distribution has been assessed with the scintillation camera using inert radioactive gases, i.e., ^{133}Xe and ^{81m}Kr, or aerosol-labeled with ^{131}I or ^{99m}Tc (3). These nuclear imaging techniques are still the primary clinical methods to determine regional ventilation abnormalities in obstructive airway diseases. Nevertheless, due to poor resolution and the complicated procedures of these techniques, most basic work on lung morphology has been performed using postmortem lung fixation and high-resolution computed tomography (4). These structural data delineate only an aerated lung and cannot be used to distinguish trapped exhaust air from fresh air in the lung. To further define nonventilated (abnormal) regions within the aerated lung, particularly in a constrictive state, a new technique to assess ventilation distribution as well as lung structure is required.

Hyperpolarized (HP) ^{3}He MRI has been shown to provide an alternative nonradioactive approach both in animals (5,6) and patients (7–11). This technique, different from more traditional ^{1}H imaging showing aerated lung structure, demonstrates ventilated regions in the lung similar to the radioactive ventilation methods described above (3). Several groups have recently demonstrated dynamic lung imaging with much-improved spatial and temporal resolution to evaluate regional pulmonary function morphologically in rats (12) and in humans (13). Previously, we incorporated a constant flow ventilator and a new scanning scheme with HP ^{3}He to acquire quantitative pulmonary images in the rat (14). We report here the use of methacholine (MCh), a provocative agonist used routinely in the clinic, to induce airway constriction in the rat. To rule out the possibility of inhomogeneous deposition within the lung by aerosol delivery, MCh was administered intravenously (i.v.). Most studies by other investigators on MCh-induced airway constriction were based on airflow and pressure measurement (15–18). This work interprets changes of lung function using a combination of the ventilation data from HP ^{3}He imaging and the structural data from conventional ^{1}H imaging in a carefully controlled animal model.

MATERIALS AND METHODS

Animal Preparation

A total of 24 female rats (Sprague Dawley, Charles River, Portage, MI) weighing 220–240 g were used for the MCh study, in addition to the control (physiological saline) study (n = 2). The Institutional Animal Care and Use Committee at Duke University approved all animal procedures. Anesthesia was induced using two separate intraperitoneal injections of ketamine (56 mg/kg) and diazepam (2.8 mg/kg). The rat was intubated under direct laryngoscopic visualization using a shortened catheter (Intravenous Cannula, 14GA, Sherwood Medical, Tullamore, Ireland). Within 3–5 min following induction of anesthesia, the rat was ventilated in a prone position at a rate of 72 breaths/min and a tidal volume (TV) of 8–8.5 ml/kg. To maintain anesthesia, ketamine (10 mg/ml) and diazepam (0.48 mg/ml) were continuously infused via a cannulated tail vein (26GA × 19 mm, Abbocath-T, Abbott Ireland, Sligo, Ireland). The infusion rate was adjusted (40–80 μl/min/kg) to keep the heart rate stable at ~280 beats/min. Body temperature was measured with a rectal probe and maintained at ~37°C via a warm air system.

Center for In Vivo Microscopy, Duke University Medical Center, Durham, North Carolina.

Grant sponsor: NCRR/NCI National Resource; Grant number: P41 RR05959/R24 CA 092656; Grant sponsor: NIH/NHLBI; Grant number: 2 R01 HL55348.

*Correspondence to: G. Allan Johnson, Center for In Vivo Microscopy, Box 3302, Duke University Medical Center, Durham, NC 27710. E-mail: gaj@orion.duhs.duke.edu

Received 11 March 2004; revised 24 May 2004; accepted 9 June 2004.

DOI 10.1002/mrm.20251

Published online in Wiley InterScience (www.interscience.wiley.com).

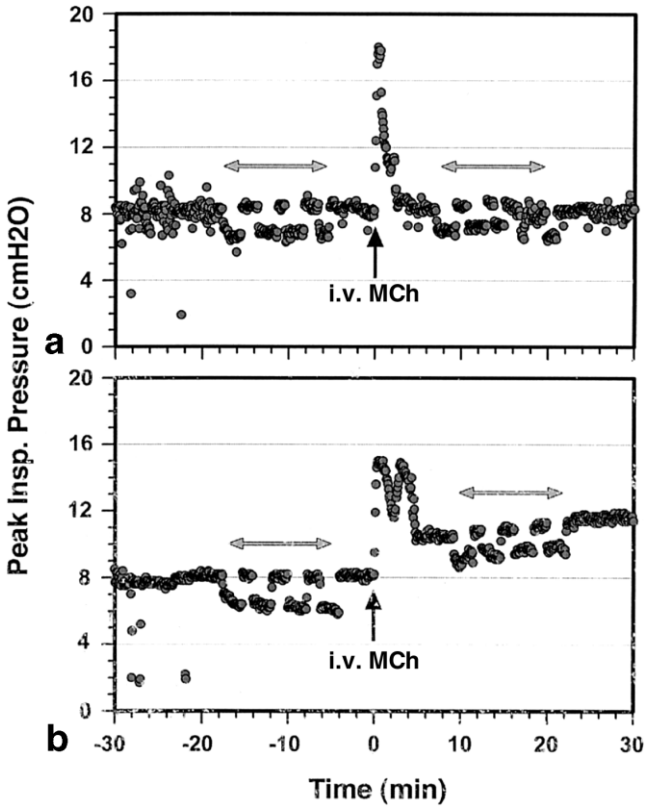

FIG. 1. Typical examples of short-reacting (**a**) and long-reacting (**b**) responses to the MCh injection (a total of 30 μg in ~0.1 ml saline). In the long-reacting case, MCh was administered with 2–3 boluses to avoid killing the rat. The TV was kept constant throughout the experiment, except for the 2-min transient period immediately after the challenge. Lung images were acquired before and after the MCh challenge as indicated (double-head arrows). The observed decreases in PIP during imaging were caused by the ^{3}He/oxygen mixed gas for ventilation.

Methacholine Administration

The MCh bolus injection (30 μg in ~0.1 ml saline) was slowly administered over 30–60 sec. Following the injection, the TV decreased as peak inspiratory pressure (PIP) increased. In preliminary experiments, the rat expired immediately when attempting to maintain the TV during this period. Because the MR signals are proportional to the amount of inhaled HP ^{3}He gas per breath, the TV was held constant throughout the study except during the 2-min period immediately following the MCh bolus injection (Fig. 1). This protocol permitted quantitative signal comparison of the ^{3}He images acquired before and after the MCh challenge. Since positive pressure ventilation was used to maintain TV, increases in airway dimensions in the ^{3}He images indicate the degree of constriction in the respective peripheral lung following the MCh challenge.

Image Acquisition and Ventilation

A 2.0 T magnet (Oxford Instruments, Oxford, UK) with shielded gradients (180 mT/m) and a Signa console (Epic 5X, GE Medical Systems, Milwaukee, WI) were used for imaging. A 7-cm-diameter birdcage RF coil was constructed to operate at 85.5 MHz and 64.8 MHz, which permitted acquisition of registered ^{1}H and ^{3}He images (6). A custom-made constant flow ventilator was used to provide a breathing pattern of a positive-pressure forced inhalation and a passive exhalation (14,19). Dynamic lung imaging was acquired during inhalation period using a ventilator-gated, 2D RA-CINE technique (12,14). The acquisition window was divided evenly into eight adjacent time frames (28.5 ms). Three different scans, described in detail previously (14), were acquired: a ^{1}H scan (flip angle = 12° and no skipping scheme) to provide anatomical landmarks of the chest, a ^{3}He scan (flip angle = 24° and no skipping scheme) focusing on the major airway branches, and a ^{3}He scan (flip angle = 12° and skip factor = 2) focusing on the lung periphery. The ^{1}H images were acquired using field of view (FOV) = 100 mm, TR = 4.75 ms, and TE = 1 ms, then regridded onto a 512 × 512 array and cropped to a 256 × 256 array covering a 50-mm FOV (14). The ^{3}He lung images were acquired using FOV = 50 mm, TR = 4.75 ms, and TE = 1 ms for a 256 × 256 array. A skipping scheme was applied: one in every second frame in the case of skip factor = 2. These imaging parameters were chosen to ensure a linear relationship between signal intensity and the flow to the regions of interest. RF spoilers were applied at the end of each breath to eliminate any residual magnetization. During the ^{3}He scans, 70% of N_2 in the inspired gas (a mixture of 23% O_2 and 77% N_2) was replaced with the HP ^{3}He gas. A total of 150 breaths were used to obtain 900 radial samples of Fourier space for each image. As illustrated in Fig. 2, coronal images were selected to cover most of the major airways. Axial images were selected at the bottom of the heart to sample more of the distal airspace. The ^{1}H and ^{3}He images, each including coronal and axial views, were acquired prior to and ~10 min after the MCh challenge.

FIG. 2. A sagittal ^{1}H image of the rat's chest demonstrates the slice selection used in this study. Coronal images (4 mm in thickness) were acquired between the two vertical lines and axial images (3 mm in thickness) were acquired between the two horizontal lines.

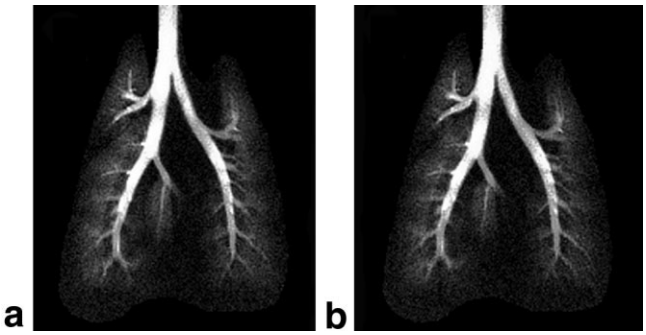

FIG. 3. The ^{3}He images at the end of inspiration are used to indicate ventilation distribution before (**a**) and after (**b**) the saline bolus injection. Images were acquired using the scan sequence identical to that used for images shown in the other figures.

Helium Hyperpolarization

A polarizer (IGI.9600.He, Amersham Health, Durham, NC) with gas capacity of ~1200 ml was used to polarize ^{3}He gas. The technique for spin-exchange optical pumping polarization has been described in detail by Happer et al. (20) and Moller et al. (21). The system achieved 30–40% nuclear polarization in 8 hr.

RESULTS

After the i.v. saline injection, PIP was unchanged. Compared to the images acquired prior to the saline injection as shown in Fig. 3, no noticeable changes in major airway size or peripheral ventilation distribution were observed. Airway responses measured by airway pressure after a bolus (~0.1 ml) of i.v. MCh (30 μg) are shown in Fig. 1. The reactivity varied between rats. Two main patterns of changes in PIP were observed (Fig. 1a,b).

In a short-reacting case (Fig. 1a), the PIP increased up to ~120% as the TV decreased by ~30% immediately after the MCh challenge. The rapid changes in the PIP and the TV diminished within 2 min. This pattern of response was observed in 20 of the 24 total MCh-tested rats with various degrees of constriction. Serial coronal ^{3}He images before and after the MCh challenge in this pattern are shown in Fig. 4. Despite the fact that the post-MCh images were acquired after the PIP returned to the baseline value (Fig. 1), inhomogeneous ventilation distribution was observed in the post-MCh coronal images (Fig. 4e–h) as compared to the pre-MCh coronal images (Fig. 4a–d). Similar results were also observed in the axial images (Fig. 5).

In a long-reacting case (Fig. 1b), PIP increased rapidly up to ~100% as the TV decreased by >50% after the MCh injection, but remained ~25% above the baseline value after the primary constriction. It appears that these rats were hyperreactive to MCh, even though these rats had not been previously sensitized. As shown in Fig. 6, a significantly increased portion of inspired air was confined in the major airway branches as the TV was maintained at the same rate. Note that some of inspired air reaching the peripheral lung was not observed in the selected coronal images since the slice thickness was only 4 mm. Major airway branches were expanded up to 2–3 times and delay in inspired airflow (Fig. 6e–h) was consistent with the increase in PIP (Fig. 1b), suggesting severe airway constriction. As the anatomical dead space increased after severe constriction (Fig. 6), the rat was hypoventilated using the same TV. Efforts to maintain oxygenation using a larger TV

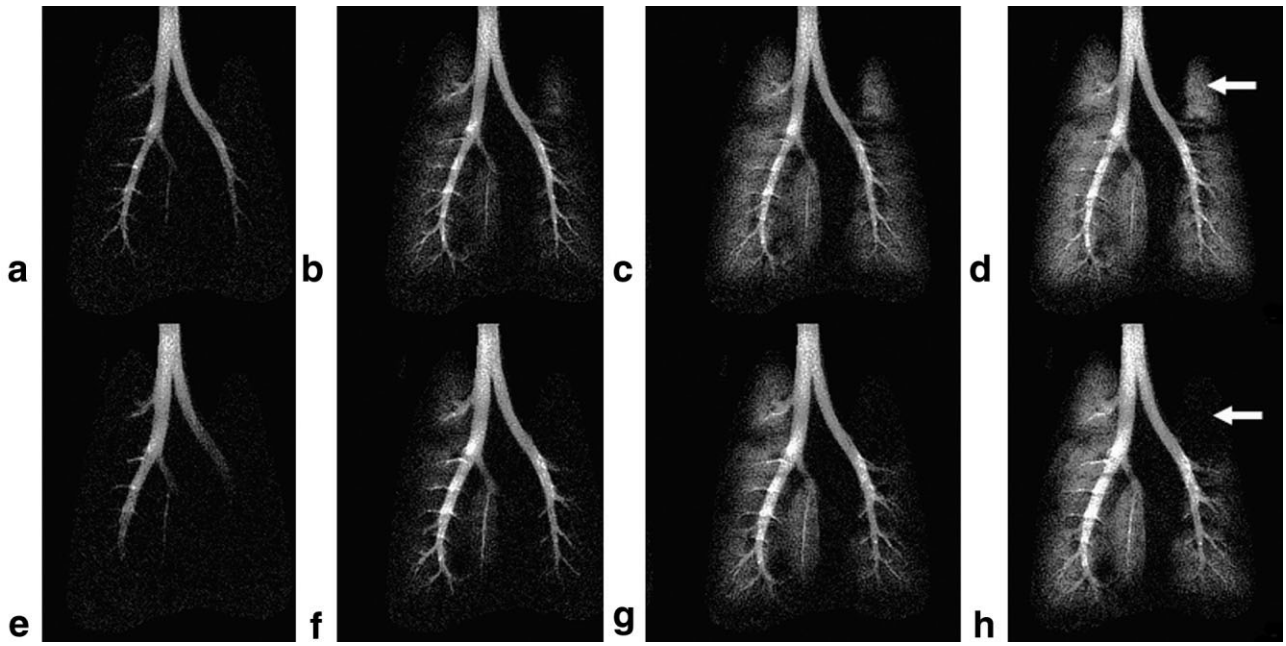

FIG. 4. Serial inspired coronal ^{3}He images (at 57 ms intervals) in the short-reacting airway response after the MCh challenge are shown. As compared with the pre-MCh images (**a–d**), delay of the inspired airflow and increases in the airway size were noticeable in the post-MCh images (**e–h**). Ventilation deficiency was observed in the regions indicated (arrows). These images provide direct evidence of heterogeneous constriction induced by MCh.

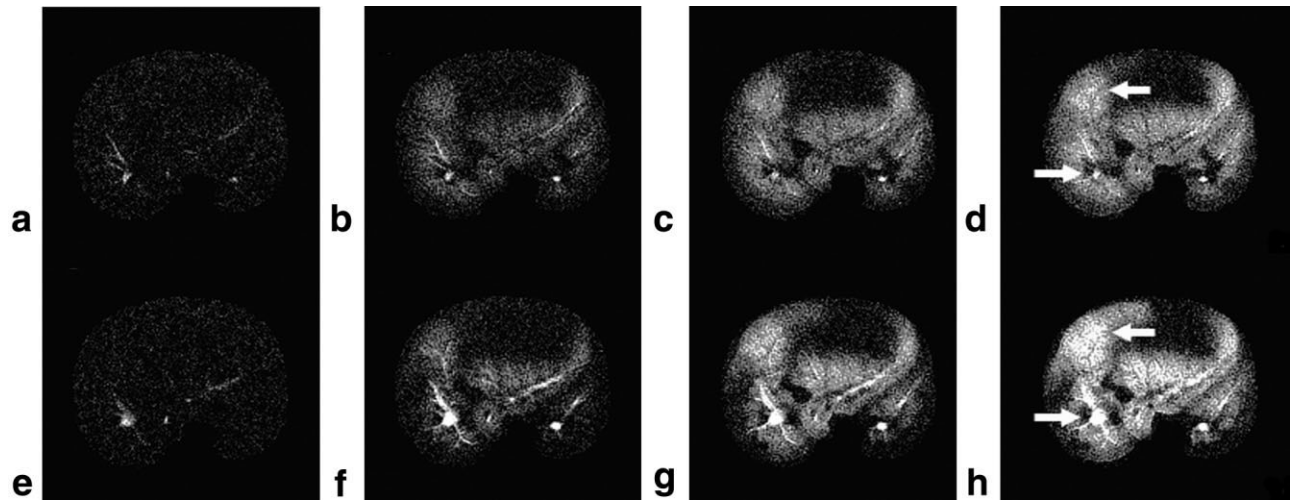

FIG. 5. Serial axial inspired ^{3}He images (at 57 ms intervals) in the short-reacting airway response after the MCh challenge are shown. As compared with the pre-MCh images (**a–d**), much brighter signals were detected in the peripheral regions marked with arrows in the post-MCh images (**e–h**). These data demonstrate that more inspired air was distributed into the regions indicated after the MCh challenge.

resulted in a pneumothorax. Four of the 24 total MCh-tested rats reacted in this fashion and died within 60 min.

An increase in lung patency after the MCh challenge was observed in the ^{1}H images in the example of short-reacting airway response (Fig. 7). These data suggest air trapped inside the lung, as reported by high-resolution computed tomography (4). The site of air trapping in the upper-left lobe of the lung can be seen in the combined ^{1}H/^{3}He coronal lung images (Fig. 7b vs. 7a). Also, the images showed more air shunting into the less-constricted right lung. These data demonstrate heterogeneous constriction induced by the i.v. MCh bolus injection.

DISCUSSION

We have demonstrated direct visualization of heterogeneous constriction induced by i.v. MCh bolus injection in the rat. Although the degree of constriction after the MCh challenge varied between rats, inhomogeneous ^{3}He distribution in the peripheral lung was observed in both pat-

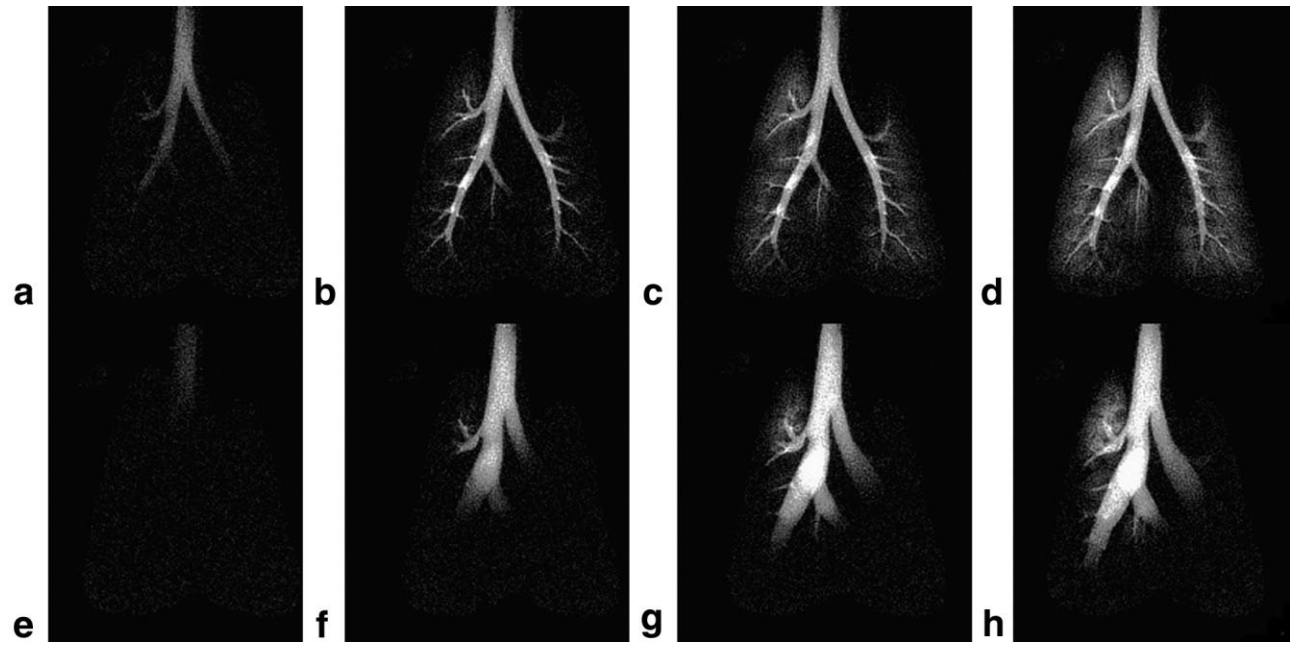

FIG. 6. Serial coronal ^{3}He images (at 57 ms intervals) in the long-reacting airway response for pre- (**a–d**) and post- (**e–h**) MCh exposure are demonstrated. Distended major airways and lack of ventilation within the peripheral regions were observed in the post-MCh images, suggesting constriction of the small airways (after the first two major airways). These data are consistent with the increase in the PIP during the imaging period, as shown in Fig. 1.

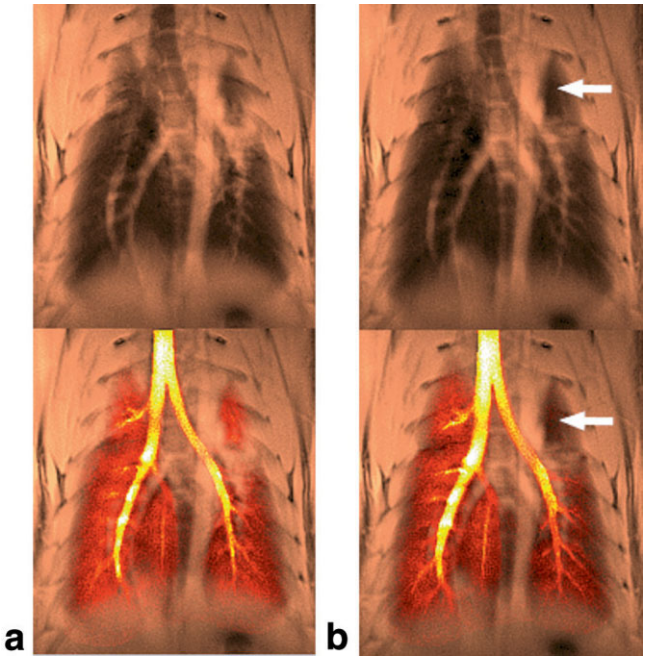

FIG. 7. Coronal comparison of the pre-MCh images (**a**) and the post-MCh images (**b**) in the case of short-reacting airway response after the MCh challenge. All images were acquired at end of inspiration. The ^{1}H lung images (top) indicate air content and the registered ^{1}H/^{3}He lung images (bottom) demonstrate ventilation distribution. After the MCh challenge, an increase in air content was observed in the upper left lobe as indicated (arrow in the top right figure), but no fresh air was distributed in the same region as marked (arrow in the bottom right figure). These combined data provide a direct visualization to locate site of lung dysfunction.

terns (Fig. 4–7). The combined ^{1}H/^{3}He lung images indicate that the airways respond to heterogeneous constriction in a fashion similar to that described by Laplace's relationship, which relates the stability between adjacent alveoli. As the MCh altered the balance between the inflated pressures of each lobe, the inspired air shunted from the more-constricted regions to the less-constricted regions. Consequently, partial/complete airway closure and air trapping occurred in the more-constricted regions, as well as overinflation in the less-constricted regions (Fig. 7b).

Inhomogeneous ventilation distribution was observed 10–16 min after the MCh challenge in the case of short-reacting airway response (Figs. 4, 5, and 7), whereas PIP returned to the baseline value within 2 min after the MCh injection (Fig. 1a). These data indicate the traditional airway pressure measurements only describe the whole lung function. Regional lung conditions did not return to the prechallenged condition as the airway pressure suggested. It is unclear whether the local constricted lung still reacted to the MCh challenge 10–16 min after the injection or the lung remained constricted until deep inspirations to reopen the airways (22). In one of our preliminary experiments (not included), we observed that the lung recovered completely 60 min after an MCh bolus injection. Further studies are required to delineate the mechanisms triggering the recovery after constriction.

Airway closure has been suggested to occur after MCh challenge. Brown et al. (23) showed that airway closure could occur even at relatively high peak end-expiration pressure. Wright et al. (24) also reported that the MCh-induced constrictions occurred primarily in the medium- and larger-sized bronchioles (>0.32 mm) using lung explants in rats. A decrease in lung density, an indicator of air content, was observed by using computed tomography after the MCh challenge (4). Yet the observed decrease in lung density could only suggest occurrences of air trapping. To locate the sites of action, we compared the ^{1}H images as an indicator of air content in the lung (patency) with the ^{3}He images as an indicator of ventilated regions. As shown in the registered ^{1}H and ^{3}He images in Fig. 7, the left upper lobe was not ventilated, but remained aerated after MCh challenge. Compared with the pre-MCh ^{1}H images (top, Fig. 7a), the post-MCh ^{1}H images (top, Fig. 7b) show an increase of air content in the upper left lobe. Since static lung elastic recoil increased after the constrictor stimuli (25), to keep the aerated region from shrinking in the constrictive state, the small airways must close partially or completely. The combined in vivo images shown here indicate partial/complete airway closure in the lung after the MCh challenge. Our results are consistent with a model proposed by Anafi and Wilson (26), which describes constriction heterogeneity as two stable states of airways—one effectively open and one nearly closed. This model provided an excellent rationale to explain the dependence of airway constriction on the TV and the peak end-expiration pressure (27–30).

In our previous study, we demonstrated that the airflow (velocity) in the major airways is proportional to the signal intensity normalized with projected airway diameter, as shown in the coronal ^{3}He dynamic images (14). In the current study, we investigated the airflow profile within the conducting airway after the MCh challenge (Table 1). The signal intensities in the regions of the trachea (M1), the right major airway branch (M2R), and the left major airway branch (M2L) were measured at the end of inhalation and were normalized with respect to the projected airway diameter for comparisons (Table 1). In a control experiment after saline injection, the airway diameter remained unchanged, but there was a trend of decrease in the normalized signal intensity (NSI), which averaged ~14% in the M1, M2R, and M2L. Since the two scans were ~30 min apart, this decrease was mainly caused by the T_1 decay of the polarization. In a short-reacting example (Table 1), the NSI in M1, M2R, and M2L increased by an average of ~6%, and the airway size decreased by an average of ~11% after the MCh challenge. A similar relationship was also observed in a long-reacting example. The NSI decreased by an average of ~35% as the airway size increased by an average of ~67% (Table 1). These results suggest that, under positive pressure ventilation, the airflow in the airways decreased in response to increases of the airway diameter after the MCh challenge. Local airflow profile could be predicted using airway diameter taken from lung images.

The attractive feature of the HP ^{3}He dynamic MR imaging technique is its unique ability to define ventilating regions within the lung that cannot be assessed by post-mortem lung fixation or high-resolution computed tomog-

Table 1
Summary of Regional Function Measurement

Coronal scan		Control		Methacholine			
				Short-reacting		Long-reacting	
Challenge		Pre	Post	Pre	Post	Pre	Post
M1	D (mm)	2.5	2.5	3.5	3.5	3.1	3.9
	ΔD^2%	0		0		58%	
	SI ± SD	3830 ± 291	3391 ± 351	6452 ± 438	6002 ± 394	5028 ± 179	4568 ± 265
	NSI	1508	1335	1843	1715	1622	1171
	ΔNSI%	−11%		−7%		−28%	
	D (mm)	2.2	2.2	2.7	2.5	2.1	2.7
	ΔD^2%	0		−14%		65%	
M2R	SI ± SD	3692 ± 357	3201 ± 486	5403 ± 394	5239 ± 196	5176 ± 315	4179 ± 210
	NSI	1717	1489	2001	2096	2465	1548
	ΔNSI%	−13%		5%		−37%	
	D (mm)	1.5	1.5	2.0	1.8	1.5	2.0
	ΔD^2%	0		−19%		78%	
M2L	SI ± SD	2715 ± 334	2253 ± 210	3943 ± 246	4264 ± 341	4241 ± 236	3453 ± 209
	NSI	1834	1522	1972	2369	2827	1726
	ΔNSI%	−17%		20%		−39%	
BG Noise		422 ± 189	413 ± 222	471 ± 267	431 ± 207	375 ± 210	404 ± 174

The regions of interest located in trachea (M1), the right major airway branch (M2R), and the left major airway branch (M2L) were selected for analysis. D: the projected airway diameter; ΔD^2%: changes of airway cross-section in percentage after the MCh challenge; SI: signal intensity; NSI: the SI normalized with the projected airway diameter; ΔNSI%: changes of the NSI in percentage after the MCh challenge; BG: the background.

raphy. The data shown here allow a direct in vivo visualization of dynamic lung morphology, as well as a quantitative measurement of local airflow in the airways. Heterogeneous bronchoconstriction after the i.v. MCh injection, resulting in partial/complete airway closure, air trapping, and ventilation redistribution, are evident using this technique. These data also suggest a lung model partitioning the lung into ventilating and nonventilating regions. Such a lung model could facilitate the interpretation of the pulmonary data measured by the airflow and airway pressure, particularly in the constricted state. Furthermore, the regional airflow in the major airway is shown to be inversely related to the respective airway size. Dynamic morphological data obtained by HP ^{3}He imaging clearly offer great advantages over traditional methods to investigate pulmonary disease models, especially in small animals. With comparable spatial (190 μm) and temporal resolution (28.5 ms), regional measurements can be assessed. Work now under way to extend these methods to specific genotypes in the mouse will allow a much deeper understanding of the underlying mechanisms of asthma.

ACKNOWLEDGMENTS

The authors thank Ted Wheeler and Gary Cofer for technical assistance, and Dr. Laurence Hedlund for helpful discussion and advice. This work was performed at the Duke Center for In Vivo Microscopy.

REFERENCES

1. Barnes PJ. Update on asthma. Isr Med Assoc J 2003;5:68–72.
2. Lemanske J, Robert F, Busse WW. Asthma. J Allergy Clin Immunol 2003;111:S502–519.
3. Taplin GV, Chopra SK. Inhalation lung imaging with radioactive aerosols and gases. Prog Nucl Med 1978;5:119–143.
4. Amirav I, Kramer SS, Grunstein MM. Methacholine-induced temporal changes in airway geometry and lung density by CT. Chest 2001;119: 1878–1885.
5. Middleton H, Black R, Saam B, Cates G, Cofer G, Guenther B, Happer W, Hedlund L, Johnson G, Juvan K, Swartz J. MR imaging with hyperpolarized He-3 gas. Magn Reson Med 1995;33:271–275.
6. Johnson GA, Cofer GP, Hedlund LW, Maronpot RR, Suddarth SA. Registered ^{1}H and ^{3}He magnetic resonance microscopy images of the lung. Magn Reson Med 2001;45:365–370.
7. MacFall JR, Charles HC, Black RD, Middleton H, Swartz J, Saam B, Dreihuys B, Erickson C, Happer W, Cates G, Johnson GA, Ravin CE. Human lung air spaces: potential for MR imaging with hyperpolarized He-3. Radiology 1996;200:553–558.
8. Kauczor H-U, Hofmann D, Kreitner K-F, Nilgens H, Surkau R, Heil W, Potthast A, Knopp MV, Otten EW, Thelen M. Normal and abnormal pulmonary ventilation: visualization at hyperpolarized He-3 MR imaging. Radiology 1996;201:564–568.
9. Donnelly LF, MacFall JR, McAdams HP, Majure JM, Smith J, Frush DP, Bogonad P, Charles HC, Ravin CE. Cystic fibrosis: combined hyperpolarized 3He-enhanced and conventional proton MR imaging in the lung—preliminary observations. Radiology 1999;212:885–889.
10. Altes TA, Powers PL, Knight-Scott J, Rakes G, Platts-Mills TA, de Lange EE, Alford BA, Mugler JP 3rd, Brookeman JR. Hyperpolarized 3He MR lung ventilation imaging in asthmatics: preliminary findings. J Magn Reson Imag 2001;13:378–384.
11. Samee S, Altes T, Powers P, de Lange EE, Knight-Scott J, Rakes G, Mugler JP 3rd, Ciambotti JM, Alford BA, Brookeman JR, Platts-Mills TA. Imaging the lungs in asthmatic patients by using hyperpolarized helium-3 magnetic resonance: assessment of response to methacholine and exercise challenge [Comment]. J Allergy Clin Immunol 2003;111: 1205–1211.
12. Viallon M, Cofer GP, Suddarth SA, Möller H, Chen XJ, Chawla MS, Hedlund LW, Crémillieux Y, Johnson GA. Functional MR microscopy of the lung with hyperpolarized ^{3}He. Magn Reson Med 1999;41:787–792.
13. Salerno M, Altes TA, Mugler JP 3rd, Nakatsu M, Hatabu H, de Lange EE. Hyperpolarized noble gas MR imaging of the lung: potential clinical applications. Eur J Radiol 2001;40:33–44.

14. Chen BT, Brau ACS, Johnson GA. Measurement of regional lung function in rats using hyperpolarized 3Helium dynamic MRI. Magn Reson Med 2003;49:78–88.
15. Hantos Z, Daroczy B, Suki B, Nagy S, Fredberg JJ. Input impedance and peripheral inhomogeneity of dog lungs. J Appl Physiol 1992;72:168–178.
16. Sato J, Suki B, Davey BL, Bates JH. Effect of methacholine on low-frequency mechanics of canine airways and lung tissue. J Appl Physiol 1993;75:55–62.
17. Nagase T, Moretto A, Ludwig MS. Airway and tissue behavior during induced constriction in rats: intravenous vs. aerosol administration. J Appl Physiol 1994;76:830–838.
18. Sakai H, Ingenito EP, Mora R, Abbay S, Cavalcante FS, Lutchen KR, Suki B. Hysteresivity of the lung and tissue strip in the normal rat: effects of heterogeneities. J Appl Physiol 2001;91:737–747.
19. Volgyesi GA, Tremblay LN, Webster P, Zamel N, Slutsky AS. A new ventilator for monitoring lung mechanics in small animals. J Appl Physiol 2000;89:413–421.
20. Happer W, Miron E, Schaefer S, Schreiber D, Wijngaarden W, Zeng X. Polarization of the nuclear spins of noble-gas atoms by spin exchange with optically pumped alkali-metal atoms. Phys Rev A 1984;29:3092–3110.
21. Moller HE, Chen XJ, Saam B, Hagspiel KD, Johnson GA, Altes TA, de Lange EE, Kauczor HU. MRI of the lungs using hyperpolarized noble gases. Magn Reson Med 2002;47:1029–1051.
22. Lauzon A, Bates J. Kinetics of respiratory system elastance after airway challenge in dogs. J Appl Physiol 2000;89:2023–2029.
23. Brown RH, Mitzner W. Airway closure with high PEEP in vivo. J Appl Physiol 2000;89:956–960.
24. Wright JL, Sun JP, Churg A. Site of methacholine reactivity in the peripheral airways: analysis using lung explants. Am J Physiol 1997; 16:L68–L72.
25. Bates JH, Lauzon AM, Dechman GS, Maksym GN, Schuessler TF. Temporal dynamics of pulmonary response to intravenous histamine in dogs: effects of dose and lung volume. J Appl Physiol 1994;76:616–626.
26. Anafi RC, Wilson TA. Airway stability and heterogeneity in the constricted lung. J Appl Physiol 2001;91:1185–1192.
27. Ding DJ, Martin JG, Macklem PT. Effects of lung volume on maximal methacholine-induced bronchoconstriction in normal humans. J Appl Physiol 1987;62:1324–1330.
28. Ludwig MS, Dreshaj I, Solway J, Munoz A, Ingham RHJ. Partitioning of pulmonary resistance during constriction in the dog: effects of volume history. J Appl Physiol 1987;62:807–815.
29. Sly PD, Brown KA, Bates JH, Macklem PT, Milic-Emili J, Martin JG. Effect of lung volume on interrupter resistance in cats challenged with methacholine. J Appl Physiol 1988;64:360–366.
30. Balassy Z, Mishima M, Bates JH. Changes in regional lung impedance after intravenous histamine bolus in dogs: effects of lung volume. J Appl Physiol 1995;78:875–880.